ESI

Enhancement of Elastohydrodynamic Friction by Elastic Hysteresis in a Periodic Structure

1. Data From Lubricated Sliding Experiments:

Samples were tested twice for each velocity and load condition, with lubricant removed between the two experiments. For each experiment two cycles were obtained, resulting in four total cycles. Friction results for each cycle were averaged to obtain the lubricated sliding friction value. Tables containing the results are provided below. Friction error was calculated using standard deviation on the data set, and error propagation was utilized for carrying error through calculations.

Table S1: Friction values for Compliant Control, R=2mm.

Compliant Control, R=2mm Friction (mN)		velocity (mm/s)								
		0.025	**0.05**	**0.1**	**0.25**	**0.4**	**0.5**	**0.6**	**0.8**	**1**
load	**18.6**	0.43	0.55	0.71	1.09	1.31	1.53	1.60	1.82	2.06
mN	**51.0**	1.06	1.30	1.55	2.26	2.73	2.89	3.15	3.46	3.83
	80.4	1.74	2.02	2.57	3.56	4.19	4.61	4.91	5.49	5.96
	113.3	2.47	2.78	3.49	4.76	5.44	6.10	6.51	7.26	7.87
	143.6	3.37	3.62	4.43	5.94	6.80	7.47	7.98	8.93	9.51
	177.0	4.60	4.80	5.74	7.42	8.49	9.32	10.24	11.32	12.15
	208.9	6.14	5.95	7.11	9.18	10.13	11.44	12.07	13.28	14.27
	238.1	8.31	7.55	8.62	10.92	11.96	13.33	13.80	15.04	15.92

Table S2: Friction error values for Compliant Control, R=2mm.

Compliant Control, R=2mm Friction Error (mN)		velocity (mm/s)								
		0.025	**0.05**	**0.1**	**0.25**	**0.4**	**0.5**	**0.6**	**0.8**	**1**
load	**18.6**	0.02	0.02	0.03	0.02	0.03	0.03	0.02	0.02	0.02
mN	**51.0**	0.02	0.03	0.03	0.06	0.04	0.03	0.02	0.03	0.05
	80.4	0.02	0.01	0.02	0.02	0.05	0.03	0.02	0.01	0.02
	113.3	0.03	0.02	0.02	0.02	0.04	0.01	0.01	0.01	0.01
	143.6	0.03	0.03	0.02	0.01	0.07	0.02	0.07	0.10	0.04
	177.0	0.02	0.02	0.08	0.14	0.02	0.19	0.03	0.01	0.02
	208.9	0.03	0.07	0.10	0.10	0.08	0.13	0.12	0.13	0.15
	238.1	0.10	0.10	0.15	0.15	0.25	0.16	0.11	0.09	0.04

Table S3: Friction values for Stiff Control, R=2mm.

Stiff Control, R=2mm Friction (mN)		velocity (mm/s) 0.025	0.05	0.1	0.25	0.4	0.5	0.6	0.8	1
load mN	18.6	0.19	0.25	0.36	0.62	0.80	0.93	1.07	1.28	1.48
	51.0	0.42	0.63	0.80	1.23	1.51	1.74	1.90	2.20	2.45
	80.4	0.60	0.78	1.04	1.58	1.96	2.16	2.42	2.76	3.08
	113.3	0.83	1.05	1.42	2.06	2.61	2.89	3.13	3.61	3.98
	143.6	1.16	1.45	1.84	2.67	3.28	3.61	3.91	4.39	4.72
	177.0	1.26	1.55	2.04	2.98	3.66	4.09	4.40	5.01	5.51
	208.9	1.79	2.16	2.69	3.71	4.45	4.88	5.21	5.86	6.39
	238.1	1.89	2.31	2.98	4.22	5.00	5.55	5.94	6.67	7.32

Table S4: Friction error values for Stiff Control, R=2mm.

Stiff Control, R=2mm Friction Error (mN)		velocity (mm/s) 0.025	0.05	0.1	0.25	0.4	0.5	0.6	0.8	1
load mN	18.6	0.006	0.02	0.02	0.005	0.01	0.01	0.01	0.02	0.01
	51.0	0.01	0.01	0.03	0.04	0.02	0.05	0.05	0.04	0.05
	80.4	0.02	0.02	0.03	0.02	0.01	0.03	0.02	0.02	0.04
	113.3	0.03	0.02	0.01	0.03	0.02	0.03	0.04	0.03	0.04
	143.6	0.05	0.04	0.01	0.02	0.06	0.02	0.03	0.01	0.09
	177.0	0.04	0.05	0.05	0.07	0.03	0.04	0.05	0.05	0.06
	208.9	0.12	0.10	0.06	0.04	0.06	0.03	0.01	0.02	0.03
	238.1	0.02	0.01	0.03	0.04	0.05	0.02	0.04	0.01	0.03

Table S5: Friction values for TPPS, R=2mm.

TPPS, R=2mm Friction (mN)		velocity (mm/s) 0.025	0.05	0.1	0.25	0.4	0.5	0.6	0.8	1
load mN	18.6	0.6	0.7	0.9	1.4	1.8	2.0	2.2	2.6	2.9
	51.0	1.9	2.1	2.6	3.8	5.0	5.0	4.0	5.9	6.4
	80.4	3.2	3.5	4.1	5.6	7.1	7.3	7.6	8.5	9.1
	113.3	4.2	4.6	5.6	7.9	9.3	9.9	10.4	11.6	12.7
	143.6	5.5	5.7	6.8	9.6	11.6	12.8	13.8	15.2	16.9
	177.0	6.8	7.0	8.5	11.8	14.2	15.8	16.7	18.8	20.5
	208.9	7.7	8.0	9.9	13.9	17.0	18.6	19.6	22.2	23.6
	238.1	9.8	10.0	11.9	16.4	19.5	21.4	22.9	25.5	27.5

Table S6: Friction error values for TPPS, R=2mm.

TPPS, R=2mm Friction Error (mN)		velocity (mm/s)								
		0.025	**0.05**	**0.1**	**0.25**	**0.4**	**0.5**	**0.6**	**0.8**	**1**
load	**18.6**	0.02	0.02	0.04	0.04	0.02	0.1	0.1	0.1	0.1
mN	**51.0**	0.02	0.05	0.1	0.1	0.2	0.1	0.5	0.2	0.2
	80.4	0.2	0.3	0.2	0.1	0.2	0.1	0.1	0.1	0.1
	113.3	0.1	0.1	0.1	0.1	0.2	0.1	0.1	0.03	0.1
	143.6	0.1	0.2	0.1	0.1	0.03	0.1	0.3	0.1	0.3
	177.0	0.2	0.2	0.1	0.01	0.1	0.1	0.2	0.3	0.1
	208.9	0.1	0.1	0.1	0.1	0.2	0.2	0.3	0.3	0.2
	238.1	0.3	0.2	0.1	0.1	0.2	0.1	0.2	0.2	0.2

Table S7: TPPS enhancement ratio, R=2mm.

TPPS, R=2mm Enhancement Ratio		velocity (mm/s)								
		0.025	**0.05**	**0.1**	**0.25**	**0.4**	**0.5**	**0.6**	**0.8**	**1**
load	**18.6**	1.9	1.8	1.8	1.7	1.8	1.7	1.7	1.7	1.7
mN	**51.0**	2.8	2.3	2.4	2.3	2.5	2.3	1.7	2.2	2.1
	80.4	3.0	2.7	2.5	2.4	2.5	2.3	2.2	2.2	2.1
	113.3	2.9	2.6	2.5	2.5	2.5	2.4	2.3	2.3	2.3
	143.6	2.7	2.5	2.4	2.4	2.5	2.5	2.5	2.4	2.6
	177.0	2.6	2.5	2.4	2.5	2.5	2.6	2.5	2.5	2.5
	208.9	2.2	2.2	2.2	2.4	2.5	2.5	2.5	2.5	2.5
	238.1	2.2	2.3	2.3	2.4	2.5	2.5	2.5	2.5	2.6

Table S8: TPPS enhancement ratio error, R=2mm.

TPPS, R=2mm Enhancement Ratio Error		velocity (mm/s)								
		0.025	**0.05**	**0.1**	**0.25**	**0.4**	**0.5**	**0.6**	**0.8**	**1**
load	**18.6**	0.1	0.1	0.1	0.1	0.03	0.05	0.04	0.05	0.04
mN	**51.0**	0.05	0.1	0.1	0.1	0.1	0.1	0.2	0.1	0.1
	80.4	0.2	0.2	0.1	0.1	0.1	0.04	0.04	0.03	0.02
	113.3	0.1	0.1	0.03	0.03	0.1	0.02	0.03	0.01	0.02
	143.6	0.1	0.1	0.05	0.02	0.03	0.01	0.1	0.03	0.1
	177.0	0.1	0.1	0.04	0.04	0.02	0.04	0.03	0.04	0.02
	208.9	0.1	0.05	0.03	0.03	0.03	0.03	0.04	0.04	0.03
	238.1	0.1	0.1	0.03	0.03	0.04	0.02	0.03	0.02	0.02

Table S9: Friction and error values for Compliant Control, R=0.5mm.

Compliant Control, R=0.5mm Friction (mN)		velocity (mm/s) 0.1	0.5	1	Compliant Control, R=0.5mm Friction Error (mN)		velocity (mm/s) 0.1	0.5	1
load mN	18.6	1.06	1.50	2.46	load mN	18.6	0.05	0.56	0.03
	51.0	4.63	5.94	7.36		51.0	0.04	0.12	0.07
	80.4	13.16	12.27	14.29		80.4	0.16	0.11	0.05
	113.3	31.22	24.43	26.64		113.3	0.24	0.16	0.21
	143.6	56.98	47.81	47.58		143.6	0.31	0.61	0.36
	177.0	92.64	82.61	81.28		177.0	0.55	0.72	0.42
	208.9	139.08	126.36	125.71		208.9	0.48	1.18	1.13
	238.1	188.86	174.49	178.75		238.1	0.48	1.20	0.40

Table S10: Friction and error values for Stiff Control, R=0.5mm.

Stiff Control, R=0.5mm Friction (mN)		velocity (mm/s) 0.1	0.5	1	Stiff Control, R=0.5mm Friction Error (mN)		velocity (mm/s) 0.1	0.5	1
load mN	18.6	0.46	0.87	1.16	load mN	18.6	0.02	0.02	0.01
	51.0	1.28	2.04	2.58		51.0	0.04	0.03	0.03
	80.4	2.03	3.16	3.92		80.4	0.01	0.01	0.01
	113.3	2.96	4.53	5.56		113.3	0.03	0.06	0.02
	143.6	4.01	5.97	7.27		143.6	0.05	0.04	0.07
	177.0	5.19	7.55	9.12		177.0	0.04	0.07	0.02
	208.9	6.51	9.20	11.12		208.9	0.07	0.09	0.07
	238.1	7.96	10.98	13.13		238.1	0.11	0.10	0.05

Table S11: Friction and error values for TPPS, R=0.5mm.

TPPS, R=0.5mm Friction (mN)		velocity (mm/s) 0.1	0.5	1	TPPS, R=0.5mm Friction Error (mN)		velocity (mm/s) 0.1	0.5	1
load mN	18.6	1.57	2.00	2.39	load mN	18.6	0.05	0.05	0.09
	51.0	4.88	5.64	6.58		51.0	0.28	0.39	0.28
	80.4	8.49	9.59	10.92		80.4	0.39	0.35	0.16
	113.3	17.39	17.18	18.18		113.3	1.21	0.40	0.79
	143.6	29.16	29.36	31.81		143.6	1.08	0.59	0.39
	177.0	48.77	42.66	44.45		177.0	6.34	0.45	0.56
	208.9	85.30	70.55	75.46		208.9	1.02	11.46	8.67
	238.1	118.10	110.87	118.18		238.1	5.96	1.57	4.87

Table S12: Enhancement ratio and error values for TPPS, R=0.5mm.

TPPS, R=0.5mm Enhancement Ratio		velocity (mm/s)			TPPS, R=0.5mm Enhancement Ratio Error		velocity (mm/s)		
		0.1	0.5	1			0.1	0.5	1
load mN	18.6	2.06	1.69	1.32	load mN	18.6	0.09	0.34	0.05
	51.0	1.65	1.41	1.32		51.0	0.10	0.10	0.06
	80.4	1.12	1.24	1.20		80.4	0.05	0.05	0.02
	113.3	1.02	1.19	1.13		113.3	0.07	0.03	0.05
	143.6	0.96	1.09	1.16		143.6	0.04	0.02	0.02
	177.0	1.00	0.95	0.98		177.0	0.13	0.01	0.01
	208.9	1.17	1.04	1.10		208.9	0.01	0.17	0.13
	238.1	1.20	1.20	1.23		238.1	0.06	0.02	0.05

Table S13: Friction and error values for Compliant Control, R=3mm.

Compliant Control, R=3mm Friction (mN)		velocity (mm/s)		Compliant Control, R=3mm Friction Error (mN)		velocity (mm/s)	
		0.05	0.4			0.05	0.4
load mN	18.6	0.53	1.44	load mN	18.6	0.02	0.02
	51	1.22	2.71		51	0.09	0.17
	143.6	2.95	5.89		143.6	0.17	0.48
	238.1	5.18	9.23		238.1	0.53	0.80

Table S14: Friction and error values for Stiff Control, R=3mm.

Stiff Control, R=3mm Friction (mN)		velocity (mm/s)		Stiff Control, R=3mm Friction Error (mN)		velocity (mm/s)	
		0.05	0.4			0.05	0.4
load mN	18.6	0.32	1.02	load mN	18.6	0.004	0.09
	51	0.62	1.69		51	0.17	0.15
	143.6	1.63	3.60		143.6	0.08	0.01
	238.1	2.48	5.24		238.1	0.16	0.06

Table S15: Friction and error values for TPPS, R=3mm.

TPPS, R=3mm Friction (mN)		velocity (mm/s)		TPPS, R=3mm Friction Error (mN)		velocity (mm/s)	
		0.05	0.4			0.05	0.4
load mN	18.6	0.99	1.85	load mN	18.6	0.10	0.05
	51	2.16	3.75		51	0.37	0.11
	143.6	5.74	9.57		143.6	0.64	0.94
	238.1	10.06	14.53		238.1	0.59	0.36

Table S16: Enhancement ratios and error values for TPPS, R=3mm.

TPPS, R=3mm Enhancement Ratio		velocity (mm/s)		TPPS, R=3mm Enhancement Ratio Error		velocity (mm/s)	
		0.05	0.4			0.05	0.4
load	18.6	2.34	1.50	load	18.6	0.11	0.08
mN	51	2.35	1.71	mN	51	0.26	0.11
	143.6	2.51	2.02		143.6	0.14	0.14
	238.1	2.63	2.01		238.1	0.15	0.11

2. Theoretical Friction Coefficient, g_E, and Lubricant Properties

In order to validate the lubricated sliding experiments, friction coefficients obtained for the control samples were compared to a theoretical model for elastohydrodynamic friction of highly compliant materials developed by Vicente et al.[1] The model defines the total friction coefficient as

$$\mu_{total} = 1.46\bar{U}^{0.65}\bar{W}^{-0.7} + SRR(3.8\bar{U}^{0.71}\bar{W}^{-0.76} + 0.96\bar{U}^{0.36}\bar{W}^{-0.11}) \quad [S1]$$

$$\bar{U} = \frac{U\eta}{E'R'} \quad [S2]$$

$$\bar{W} = \frac{W}{E'R'^2} \quad [S3]$$

where U is the sliding velocity, W is the normal load (same as our N), E' is the reduced elastic modulus, R' is the reduced radius, η is the lubricant viscosity, and SRR is the sliding to rolling ratio (2 for pure sliding). Plots in Figure S1 show the experimental and theoretical friction coefficients for the stiff control and compliant control for loads of 18.6, 113.3, and 238.1mN. We find that the theory is in good agreement for the higher modulus stiff control for all loads tested and for the low load tested for the compliant control. For the larger loads tested in the compliant control experiments the theory begins to under predict the experimental results. While the theoretical equation was developed for compliant materials, it was shown to be a good fit for materials about 2 orders of magnitude stiffer than the compliant control. Thus there could be additional mechanisms occurring in more compliant contacts that could be contributing to the friction. Overall the theory does validate the conclusion that the control experiments are providing friction values close to what is expected for compliant elastohydrodynamic lubrication.

For an isoviscous system, the parameters g_E and g_α can be used to estimate if the system is operating in the isoviscous-elastic regime[2]. If the viscosity of the fluid is independent of pressure in the experimental range tested, the pressure index α is approximately equal to zero, resulting in a g_α value of approximately zero. It has been shown experimentally at the pressures tested experimentally in the main paper, silicone oil (the main component of the lubricant used) has a viscosity independent of pressure[3]. This means the system is in either the rigid or elastic isoviscous regime. g_E is defined such that

$$g_E = V^{-2} = \left(\frac{N^4}{G\eta^3 U^3 R^5}\right)^{2/3} \qquad [S4]$$

where V is the dimensionless velocity defined in the main text of the manuscript, G is the shear modulus, N is the normal load, and R is the indenter radius. Isoviscous systems with g_E values larger than 120 are expected to be operating in the isoviscous elastic regime, with lower values putting the system into the isoviscous rigid regime. For our experiments g_E values ranged from $9.3\text{x}10^4$-$8.3\text{x}10^{11}$, putting us well into the isoviscous elastic regime.

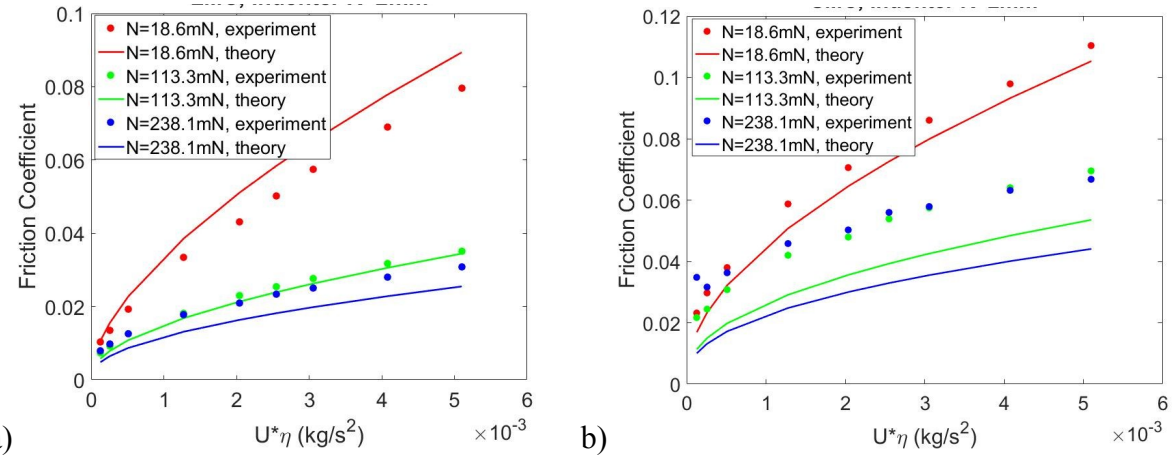

a) b)

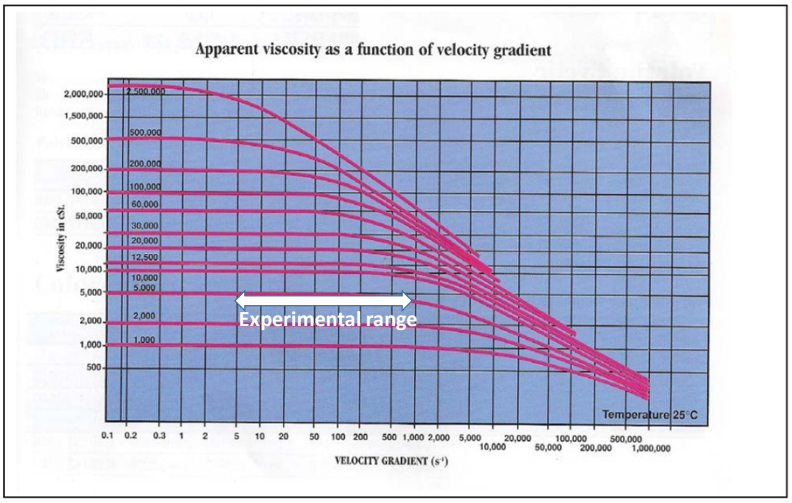

c)

Figure S1. a-b)Plots showing experimental and theoretical values of friction coefficient vs U*η for lubricated sliding with the R=2mm indenter a) Stiff control b) Compliant control. (c) Data showing silicone oil viscosity is essentially independent of shear rate in our experimental range[5].

We anticipate that the lubricant (PDMS base) will not easily slide with respect to the solid surface. This is captured by the no-slip condition that is part of the Reynolds lubrication model used to interpret our experimental data. Also, the gap between the indenter and PDMS is ~ 1

micron. The molecular weight of PDMS base is about 27000 and that of the repeat unit is 74 so there are about 365 repeat units[4]. The length of the Si-O bond is about 1.5 Angstroms, so the contour length is about 550 Angstroms. This is already much smaller than the gap between the indenter and PDMS. The radius of gyration or end-to-end rms distance will be much smaller, estimated to be between 3 and 10 nm based on Kuhn length of 1.5 – 15 Angstroms. This is clearly much smaller than the gap thickness of ~1000 nm so a continuum fluid mechanics approach is valid.

As a further check of our assumptions, we examine the rate dependence of PDMS base (primarily silicone oil) viscosity. Figure S1(c) shows that for velocity gradients in our experimental range, silicone oil viscosity is essentially independent of shear rate.

3. Lubricant Behavior Over Experimental Timescales

PDMS base was used as a lubricant as it wets the samples very well. It is a concern that PDMS base and other silicone oil based lubricants may swell PDMS over time, which could affect the measurements. Samples were coated with lubricant, tested, and then cleaned off using tape and stored dry until further testing. Samples were tested over at least two different days, after being lubricated and then cleaned and left overnight. Reproducibility of experiments was good, as shown in the errors reported. To further ensure that swelling was not affecting lubricated sliding measurements over the timescales of the experiments the compliant control and stiff control samples were tested immediately upon lubricant being placed on the surface, and then again after the lubricant had been left on for 7 hours for 3 load and velocity conditions. Tables S17 and S18 show the results of these experiments, and again reproducibility of the experiments is good.

Table S17: Timed lubricated sliding friction experiment for the compliant control

Sliding Rate	Friction					
	18.6 mN Load		113.3 mN Load		238.1 mN Load	
(mm/s)	t=0	t=7h	t=0	t=7h	t=0	t=7h
0.1	0.73	0.67	3.28	3.05	7.51	7.03
0.5	1.43	1.56	5.69	5.60	12.05	11.66
1	2.06	2.18	7.55	7.43	15.48	15.25

Table S18: Timed lubricated sliding friction experiment for the stiff control

Sliding Rate	Friction					
	18.6 mN Load		113.3 mN Load		238.1 mN Load	
(mm/s)	t=0	t=7h	t=0	t=7h	t=0	t=7h
0.1	0.45	0.47	1.61	1.58	3.36	3.10
0.5	1.11	1.09	3.05	3.13	5.78	5.71
1	1.61	1.70	4.13	4.35	7.60	7.65

4. Comparison of Periodic Force Curves for R=0.5 and R=2mm Indenters

Figure S2 shows plots for the lubricated sliding experiments under a normal load of 113.3mN and a velocity of 0.5mm/s for an indenter radius of 0.5mm in Figure S2 (a) and 2mm in Figure S2 (b). The conditions in Figure S2 (a) correspond to an enhancement ratio of 1.19 while the conditions in Figure S2 (b) correspond to an enhancement ratio of 2.4. Both the shape and magnitude of the force response for the TPPS vary between the two indenter radii, with the 0.5mm radius indenter having larger magnitudes with smaller relative gaps between the curves. The magnitude of the sliding friction for the compliant control is also significantly larger for the 0.5mm radius indenter. The larger magnitudes are likely due to the fact that under the same normal load the smaller radius indenter will be applying larger pressures to the contact region. Therefore, based on the scaling analysis from Figure 3 (b) in the main paper the 0.5mm radius indenter is no longer operating in the EHL regime for the compliant control and TPPS experiments, so intrinsic friction may be adding to the magnitude of the friction response.

Two features which stand out when comparing the force response of the 0.5 and 2mm radius indenters are the shape of the region where the force temporarily plateaus while decreasing from the peak value and the speed and duration of the force decrease. The plateau area which occurs after the initial steep decline from the peak value appears to be more substantial for the 0.5mm radius indenter. From the video analysis we know this region corresponds to the indenter being in contact with only the stiff region of the TPPS sample, so it makes sense that this would occur for a longer duration with the smaller indenter. For the 0.5mm radius indenter case, after the peak force is reached the force appears to decrease at a more rapid rate than for the larger indenter. It also decreases to a lower value relative to the centerline of the cycle curve. The fact that the force decreases more rapidly and to a lower relative value for the small indenter case compared to the larger indenter may give some additional insight to why the enhancement was only seen for larger indenter case. The energy that was dissipated from the system to achieve the periodic peaks which significantly exceed the force values for the stiff control and compliant control samples is being regained as the force value decreases below the stiff control and compliant control force values. Since this happens very quickly after the peak, and continues to very low force values for the smaller indenter case, the enhancement effect is no longer present.

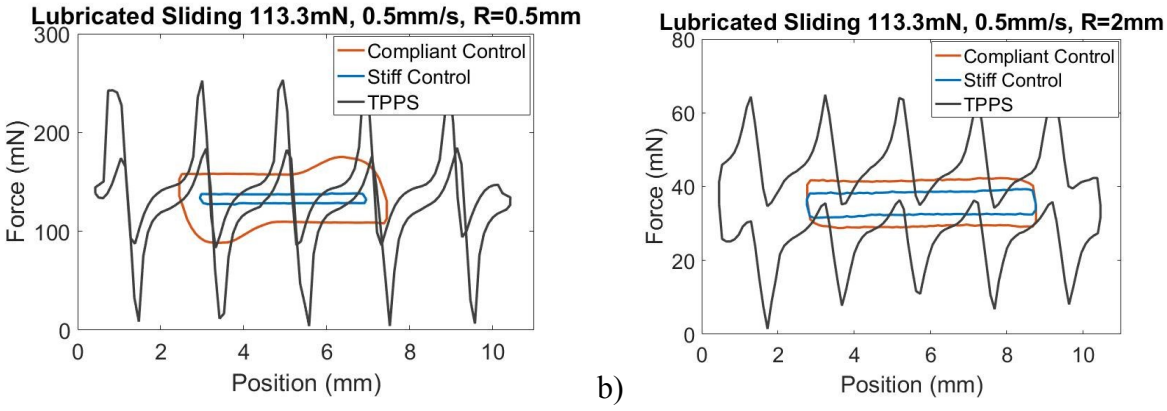

Figure S2. Plots showing force data for lubricated sliding experiments with a load of 113.3mN and velocity of 0.5mm/s for a)indenter with R=0.5mm b)indenter with R=2mm.

5. Dry Sliding Experiment

For dry sliding, preliminary experiments only focused on the results of the TPPS and the compliant control, as it was expected that the compliant control would have the largest friction of the two controls due to its larger contact area (for the same normal load). As is shown in Figure S3, under dry conditions friction force for the TPPS sample exhibits periodicity, but the peak force does not exceed values observed for the steady state sliding of the compliant control. This suggests that the higher intrinsic friction values under dry conditions dominate the overall friction behavior compared to contributions due to elastic hysteresis. It is possible for dissipative mechanisms due to structure to occur under dry conditions, but for this system if those mechanisms are occurring they are at magnitudes much smaller than the intrinsic friction, and thus no enhancement is achieved.

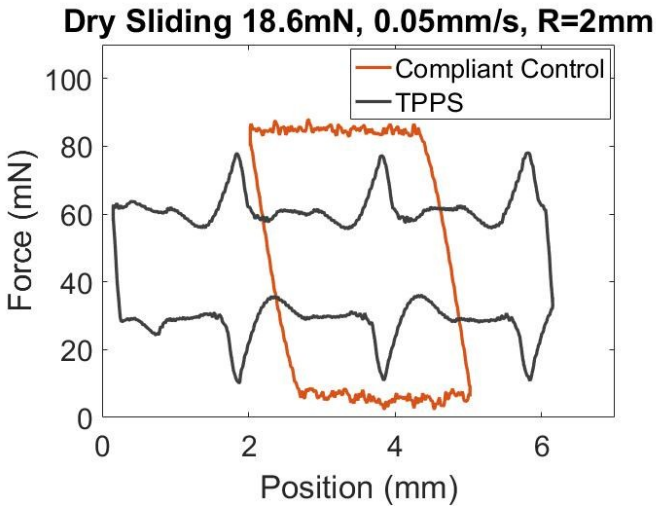

Figure S3. Plot of dry sliding friction experiment with a load of 18.6mN, velocity of 0.05mm/s, and an indenter radius of 2mm.

6. Comparison of Experimental *V* to Typical Tire Conditions

As seen in the plots in Figure 3 in the main paper, the normalized velocities, *V*, tested experimentally range from about $V=10^{-4}$-10^{-7}. Table S19 shows estimates for *V* for typical tire/road conditions, and similar magnitudes of values are obtained, suggesting results from the paper may be quite relevant to tire applications.

Table S19: Normalized velocity values, V, for typical tire conditions using a tire pressure of 10^6 N/m^2, a viscosity of 1cP (the viscosity of water), and a tire rubber shear modulus, G, of 10^6 N/m^2.

Normalized Velocity (V)	Indenter Radius						
Velocity, m/s	1.0E-06	3.2E-06	1.0E-05	3.2E-05	1.0E-04	3.2E-04	1.0E-03
0.10	2.2E-05	6.9E-06	2.2E-06	6.9E-07	2.2E-07	6.9E-08	2.2E-08
0.14	3.1E-05	9.9E-06	3.1E-06	9.9E-07	3.1E-07	9.9E-08	3.1E-08
0.21	4.5E-05	1.4E-05	4.5E-06	1.4E-06	4.5E-07	1.4E-07	4.5E-08
0.30	6.5E-05	2.1E-05	6.5E-06	2.1E-06	6.5E-07	2.1E-07	6.5E-08
0.43	9.3E-05	3.0E-05	9.3E-06	3.0E-06	9.3E-07	3.0E-07	9.3E-08
0.62	1.3E-04	4.3E-05	1.3E-05	4.3E-06	1.3E-06	4.3E-07	1.3E-07
0.89	1.9E-04	6.1E-05	1.9E-05	6.1E-06	1.9E-06	6.1E-07	1.9E-07
1.28	2.8E-04	8.8E-05	2.8E-05	8.8E-06	2.8E-06	8.8E-07	2.8E-07
1.85	4.0E-04	1.3E-04	4.0E-05	1.3E-05	4.0E-06	1.3E-06	4.0E-07
2.66	5.8E-04	1.8E-04	5.8E-05	1.8E-05	5.8E-06	1.8E-06	5.8E-07
3.19	6.9E-04	2.2E-04	6.9E-05	2.2E-05	6.9E-06	2.2E-06	6.9E-07

7. Particle Tracking Analysis

Fluorescent particles (Cospheric FMR-1.3, diameters of 1-5μm) were added to the lubricant for visualization of the flow behavior during lubricated sliding. Videos showing particle flows during experiments for the compliant control, stiff control, and TPPS are as follows:

Stiff_0p5mmps_18p6mN_FP_10x: (stiff control, U=0.5mm/s, N=18.6mN, video in real time)

Stiff_0p5mmps_113p3mN_FP_10x: (stiff control, U=0.5mm/s, N=113.3mN, video in real time)

Compliant_0p5mmps_18p6mN_FP_10x: (compliant control, U=0.5mm/s, N=18.6mN, video in real time)

TPPS_0p5mmps_18p6mN_FP_10x: (TPPS, U=0.5mm/s, N=18p6mN, video in real time)

TPPS_0p5mmps_113p3mN_FP_10x: (TPPS, U=0.5mm/s, N=1113.3mN, video in real time)

All the controls showed a similar steady state particle flow behavior. Because of the particle size there is a region in the center of contact, where the fluid film is thin, that is free of particles. This region was larger for the compliant control under the same load and velocity conditions. The TPPS videos show unsteady particle flow behavior, where the region devoid of particles changes periodically as the two phases pass under the indenter.

Particle trajectories were obtained using TrackMate, a plugin for the Fiji distribution of ImageJ.[6] For particle tracking using TrackMate, the LoG detector, along with the Simple LAP

tracker were used. Only tracks connected over at least 40 frames were accepted as particle trajectories. Particle locations for each frame were exported from the software and analyzed using MatLab. Quiver plots were made of the particle velocity vectors in each frame, and were compiled into a video mirroring the raw particle recordings. For example, the two videos indicated below are the experiment and subsequent particle velocity vector analysis for the stiff control for a velocity of 0.5mm/s and a load of 18.6mN.

stiff_0p5mmps_18p6mN_FP_10x

vel_vect_stiff_0p5mmps_18p6mN_10x

Frame by frame velocity vector videos were also compiled for the TPPS, in order to better visualize the unsteady particle flow over one period of sliding, as is seen in video

vel_vect_TPPS_0p5mmps_113p3mN_10x

where the yellow shaded region indicates the smaller modulus phase and the unmarked region indicates the larger modulus phase.

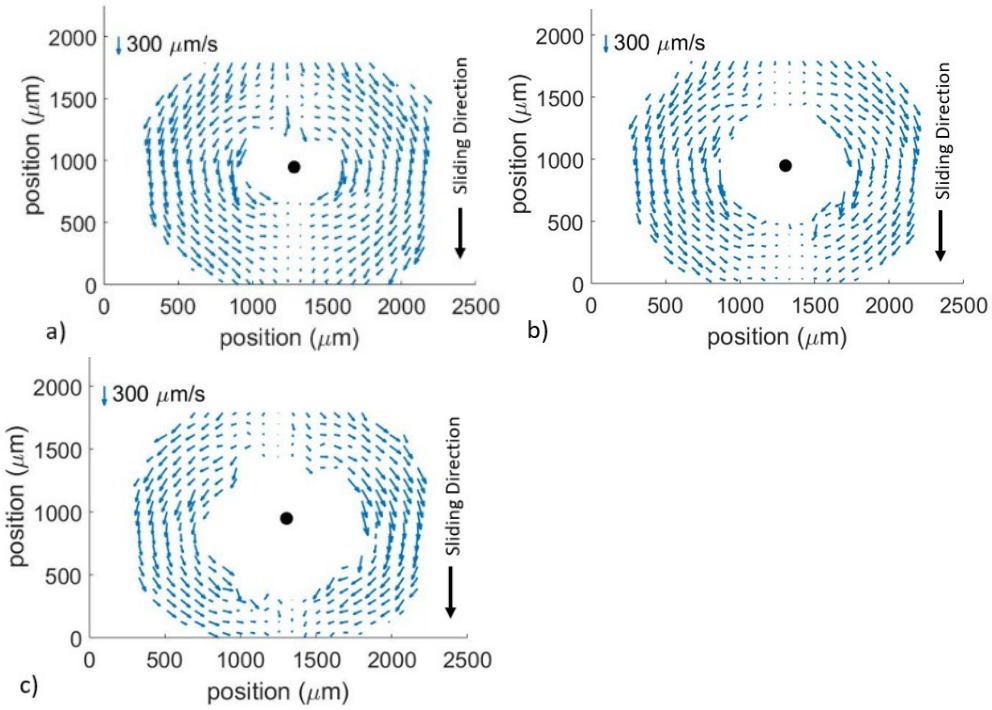

Figure S4. a) stiff control, U=0.5mm/s, N=18.6mN b) stiff control, U=0.5mm/s, N=113.3mN c) compliant control, U=0.5mm/s, N=18.6mN (particles passing through center not included in quiver plot)

For the individual frame quiver plots, when particle velocities were calculated using trajectory data from two adjacent frames the results showed fluctuations due to some error in the particle tracking trajectories, i.e. the positions traveled from frame to frame were not large enough to accurately describe particle trajectories. Thus particle velocities were obtained for each frame by

using the distance traveled over a total of 10 frames, 5 frames before and 5 frames after the designated frame. For the steady state cases it was possible to average the velocity profiles in each frame to obtain a time averaged velocity field. To do this the visualized area was divided into a square 21x21 space grid. All frames with velocity vector information were processed. Each time a frame was analyzed, any particle which was located in a certain grid had its velocity during that frame recorded and saved to the grid. On the next frame if the particle had entered a different grid then its current velocity data was now recorded to the new grid. Once all frames were analyzed, each grid had all velocities attributed to them averaged, creating a time (and film-thickness) averaged velocity field, as is shown in Figure S4 for different stiff control and compliant control experimental conditions. These velocity fields highlight the steady nature of the flow with the control samples, which is to be expected.

8. Normalized Friction and Velocity in the Compliant-Substrate Limit of Elasto-Hydrodynamic Lubrication

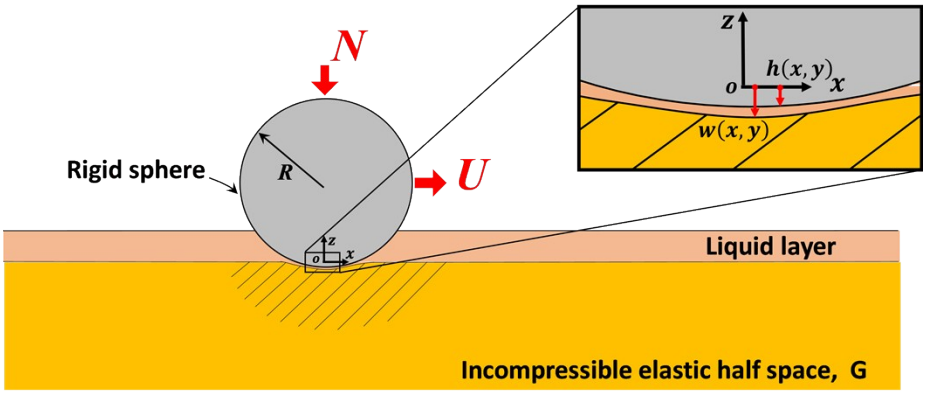

Figure S5. Schematic figure of a rigid sphere of radius R sliding steadily with velocity U on an incompressible elastic half space covered by a liquid layer. The thickness of the liquid layer between the indenter surface and the deformed substrate surface is $h-w$. (Note that for highly compliant substrates both h and w are negative and w is of the greater magnitude such that h-w is a positive number.)

Based on Reynold's lubrication theory, we show that the solution for steady sliding of a rigid sphere against an elastic half space depends on a single dimensionless parameter, $V = U\eta R^{5/3}G^{1/3}N^{-4/3}$. This parameter may be viewed as a normalized velocity in which U is the sliding velocity, η is the fluid viscosity R is the radius of the spherical indenter, G is the shear modulus of the substrate, and N is the normal load. Under these conditions, the Reynold's equation is[7,8]:

$$(p_{,x}(h-w)^3)_{,x} + (p_{,y}(h-w)^3)_{,y} = -12\eta U(h_{,x}w_{,x}) \qquad [S5]$$

where p is the fluid pressure, w is the vertical surface displacement of the substrate, h is the indentation of the sphere (see Fig. S5), and a comma denotes a partial derivative. The factor $(h-w)$ is the thickness of the fluid layer, where

$$h = h_o + \frac{x^2 + y^2}{2R}, \quad w(x,y) = -\frac{1}{4\pi G}\iint_{2D} p(x_p,y_p)[(x - x_p)^2 + (y - y_p)^2]^{-1/2} dx_p dy_p \qquad \text{[S6]}$$

Here h_0 is the position of the tip of the indenter relative to the undeformed substrate surface and is negative in the limit of Hertz-like contact. We introduce the following normalization:

$$X,Y = \frac{x,y}{a}, \quad Z = \frac{Rz}{a^2}, \quad W = \frac{Rw}{a^2}, \quad H = \frac{Rh}{a^2} = -H_o + \frac{1}{2}(X^2 + Y^2), \quad P = \frac{pR}{4\pi G a} \qquad \text{[S7]}$$

where $a = (\frac{3NR}{16G})^{1/3}$ is the Hertz radius. Using these normalized variables, (1) and (2b) become

$$[P_{,x}(H - W)^3]_{,x} + [P_{,y}(H - W)^3]_{,y} = -c_1 V(H - W)_{,x} \qquad \text{[S8a]}$$

$$W(X,Y) = -\iint_{2D} [(X - X_P)^2 + (Y - Y_P)^2]^{-\frac{1}{2}} P(X_P,Y_P) dX_P dY_P \qquad \text{[S8b]}$$

where c_1 is the constant $\frac{3}{\pi}(\frac{16}{3})^{4/3}$, and V is the dimensionless factor (dimensionless velocity) defined in the main text, eq. 3, i.e.,

$$V \equiv R^{5/3} G^{1/3} N^{-4/3} \eta U \qquad \text{[S9]}$$

In the Hertz limit, $V \to 0$. Equation (S8 a, b) implies that the normalized pressure and displacement depends only on two dimensionless parameters H_o and V. However, H_o is a function of V since the position of the indenter is determined by the normal force N. Mathematically, this can be seen from

$$N = \iint_{2D} p(x,y) dx dy \to 1 = \frac{3\pi}{4}\iint_{2D} P(X,Y,H_o,V) dX dY \to H_o = H_o(V) \qquad \text{[S10]}$$

Hence the solution of the EHL problem, that is, the normalized pressure P and displacement W, depends only on the single dimensionless parameter V.

The frictional force arises due to shear stress in the lubricant, τ, which is given in terms of the 'z' gradient of velocity, $\dot{u}_x$:

$$\tau = \eta \frac{\partial \dot{u}_x}{\partial z} \qquad \text{[S11]}$$

In Reynolds' theory, the velocity is given in terms of pressure gradient by

$$\dot{u}_x = \frac{P_{,x}}{2\eta}(z-h)(z-w) + \frac{U_1(z-w)}{h-w} \; ; \; \frac{\partial \dot{u}_x}{\partial z} = \frac{P_{,x}}{2\eta}2z - \frac{P_{,x}}{2\eta}(w+h) + \frac{U_1}{h-w} \quad \text{[S12]}$$

The frictional force is $f = \iint_A \tau dx dy$, and we evaluate it at $z=h$. Then, upon change of variables to dimensionless quantities, and using the Hertz expression for contact radius a,

$$F \equiv fR^{2/3}G^{1/3}N^{-4/3} = c_2 \iint_A [P_{,X}\frac{(H-W)}{2} + \frac{c_3 V}{(H-W)}]dXdY \quad \text{[S13]}$$

where, c_2 and c_3 are the constants $4\pi(\frac{3}{16})^{4/3}$ and $\frac{1}{4\pi}(\frac{3}{16})^{4/3}$ respectively, while $F \equiv fR^{2/3}G^{1/3}N^{-4/3}$ is a dimensionless quantity that we may call the normalized frictional force (defined in eq (5) of the main text). Equation (S13) demonstrates that normalized frictional force is determined by the same single dimensionless velocity, V. Because (H-W) is a small quantity in the Hertz limit, the first term in eq. (S13) above is negligible compared to the second term, so we can further conclude that

$$F \approx c_2 V \iint_A [\frac{1}{(H-W)}]dXdY = V\varphi(V) \quad \text{[S14]}$$

where $\varphi(V)$ is a dimensionless function of V.

9. Finite Element Simulation of Sliding Resistance Due to Elastic Ploughing

We used a finite element (FE) model to demonstrate that when a cylindrical indenter slides across a surface which is structured with a periodic pattern of varying modulus, the indenter will experience observable resistance as it approaches the boundary between compliant and stiff regions even though the overall friction is zero. The FE model and results are shown below.

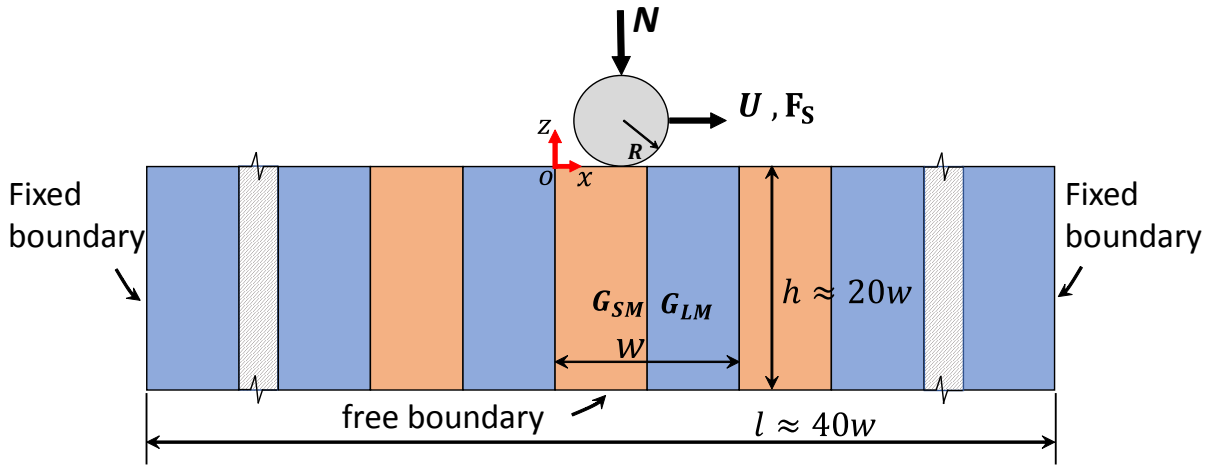

Fig.**S6** a schematic figure of a cylindrical indenter sliding on a frictionless surface structured with aperiodic pattern of varying modulus.

A schematic figure of the geometry in our FE model is shown in Fig. S6. A rigid cylinder of radius *R* indents the structured surface under a constant normal force N. The structured surface consists of alternating soft (orange) and stiff (blue) strips of equal width w/2, with different shear moduli G_{SM} and G_{LM} respectively; $G_{SM} \le G_{LM}$. The strips are assumed to be infinite in the out-of-plane direction.

The FE simulation was carried out using the commercial software package, ABAQUS®. We used a 2D plane strain model. The structured substrate was modeled with hybrid plane strain elements CPE3H and CPE4H. The built-in incompressible neo-Hookean material in ABAQUS was selected to model the substrate's mechanical behavior with a small-strain shear modulus $G_{SM} = 1MPa$ for the soft strip and the various values for shear modulus of the stiffer region. The soft and stiff regions are bonded together by 'tie' constraints. The rigid cylinder was modeled with two dimensional two-node rigid elements R2D2. The contact between the cylinder and the substrate was assumed to frictionless to highlight the effect of surface patterning on friction.

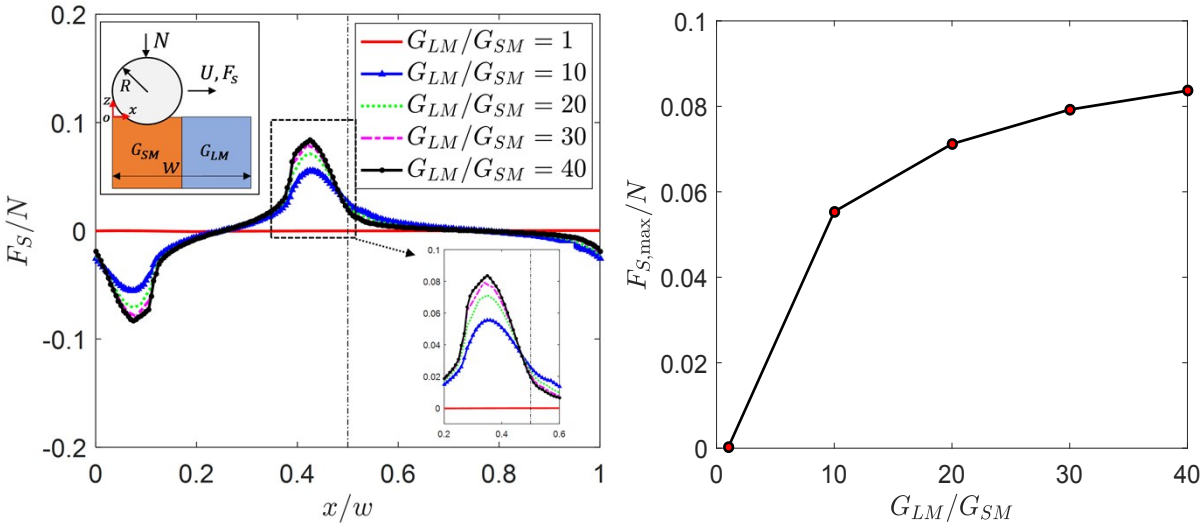

Fig.S7 (a) F_S / N varies as the cylinder slides to different positions x; frictional resistance peaks as the cylinder approaches the boundary between soft and stiff regions, $R = 2mm$, $w = 4mm$; (b) maximum ratio of F_S / N increases with increasing G_{SM} / G_{LM}.

After the cylinder was brought into contact with the structured surface under the constant normal force, its center was translated from $x = 0$ to $x = w$ (one period). The origin x = 0 is indicated in Fig.S6. The horizontal reaction force F_S required to move the cylinder varies with the position of the center of the cylinder. This force arises due to ploughing – the elastic deformation provides a force opposing motion. Dimensional analysis indicates that the reaction force F_S and its maximum $F_{S,\max}$ obey

$$F_S = N \cdot f_s\left(\frac{x}{w}, \frac{R}{w}, \frac{N}{G_{LM} R}, \frac{G_{LM}}{G_{SM}}\right) \quad \text{[S15a]}$$

$$F_{S,\max} = N \cdot f_{s\max}\left(\frac{R}{w}, \frac{N}{G_{LM} R}, \frac{G_{LM}}{G_{SM}}\right). \quad \text{[S15b]}$$

Here we focus on the effect of the ratio G_{LM} / G_{SM} on the friction force F_S. When the cylinder's center is directly above $x = 0.25w$, F_s is zero due to symmetry. As shown in Fig.S7 (a), $\pm F_{s,\max}$ occurs near the boundaries between the strips. It increases with G_{LM} / G_{SM} and vanishes when $G_{LM} / G_{SM} = 1$. *In a stable and perfectly elastic system, there is no net horizontal force since the force changes sign as the indenter moves from the stiff to soft layer.* However, it has been shown by many experiments that elastic instabilities (such as those that accompany crack trapping) can lead to dissipation even in highly elastic solids. That is, if the peak force is released unstably, it can result in loss of energy which would give rise to friction. Here we measure ratio $F_{s,\max} / N$. As shown in Fig.S7, this ratio starts at zero for a homogenous surface and increases with G_{LM} / G_{SM}. However, as argued in the main text, in our system the contribution of this effect to friction enhancement is minor.

10. Sliding Experiments Parallel to Multiphase Strips

Experiments were done where sliding friction was tested parallel to the patterned stripes (the TPPS sample was rotated 90 Degrees relative to the experiments in the main text), and a loss of enhancement occurred, as is shown in Table S20. Two positions were tested with the rotated TPPS sample, one where it was centered over the stiffer strip of material and one where it was centered over the more compliant strip of material. The results in TableS20 show that the friction values obtained sliding over the stiff and compliant strips correlate to the friction values obtained from the stiff and compliant controls. When averaged using the surface area fractions from the main paper (0.4 for the compliant material and 0.6 for the stiff material), it can be seen that these values are much less than the value obtained for sliding over the TPPS perpendicular

to the strips. This reiterates that the enhancement mechanism is dependent on the periodic change in compliance of the material.

Table S20. Comparison of experiments from paper (sliding perpendicular to patterned stripes) to rotating the TPPS sample 90 Degrees and sliding along only one phase of material(sliding parallel to patterned stripes).

	Load=51mN					
	Sliding perpendicular to patterned strips			Sliding parallel to patterned strips		
Velocity	Compliant Control	Stiff Control	TPPS	Compliant Strip	Stiff Strip	Average Force
mm/s	(mN)	(mN)	(mN)	(mN)	(mN)	(mN)
0.5	2.9	1.7	5.0	2.8	1.6	2.1
1	3.8	2.4	6.4	3.8	2.3	2.9

11. Estimate of G_{ave} for TPPS Scaling

In equations (3) and (5) from the main text, we need to provide a value of shear modulus to compute the dimensionless velocity and friction. These values are uniquely defined for the two controls. In order to compare the TPPS structure on the same plot (green circles), we need to provide an effective modulus. We can consider two limits, one in which the contact region is much larger than the structure and a second one in which it is much smaller than the structure. In the main text we have chosen the former, in which case the indenter would experience the arithmetic average of the two moduli. In the latter limit, one would use $(G_{ave})^{1/3} = 0.4(G_{SMC})^{1/3} + 0.6(G_{LMC})^{1/3}$. This results in similar scaling results and enhancements, as shown in Figure S8. The G_{ave} from the main text is the more conservative estimate.

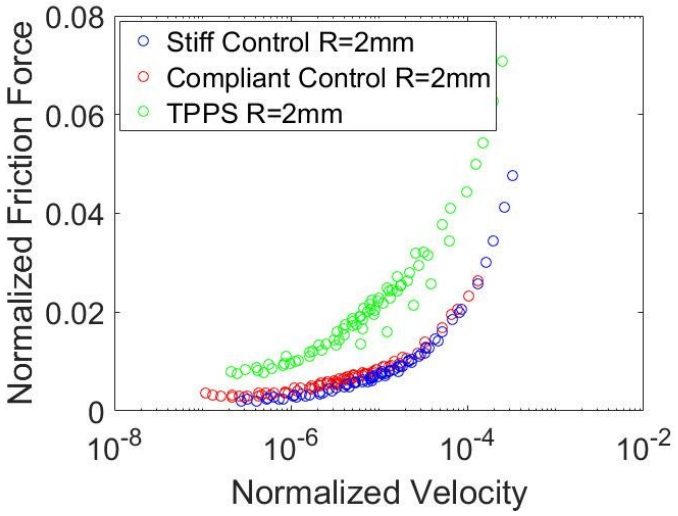

Fig. S8. Replot of Figure 3(a) from main text, but now using $(G_{ave})^{1/3} = 0.4(G_{SMC})^{1/3} + 0.6(G_{LMC})^{1/3}$ to define the average shear modulus for the TPPS.

SI References

1 J. De Vicente, J. R. Stokes and H. A. Spikes, *Tribol. Lett.*, 2005, **20**, 273–286.

2 B. N. J. Persson, *Sliding Friction : Physical Principles and Applications*, Springer, 1998.

3 W. J. Bartz and J. Ehlert, *J Lubr Technol Trans ASME*, 1976, **98**, 500–508.

4 A. Santiago-Alvarado, A. S. Cruz-Felix, F. Iturbide and B. Licona-Moran, *Int. J. Eng. Sci. Innov. Technol.*, 2014, **3**, 563–571.

5 Rhealogical Behavior of Silicone Fluids under Shear, http://www.clearcoproducts.com/pdf/library/Shear-Rhealogical.pdf.

6 J. Y. Tinevez, N. Perry, J. Schindelin, G. M. Hoopes, G. D. Reynolds, E. Laplantine, S. Y. Bednarek, S. L. Shorte and K. W. Eliceiri, *Methods*, 2017, **115**, 80–90.

7 A. (Alastair) Cameron, *Basic lubrication theory*, E. Horwood, 1976.

8 D. Dowson, G. R. Higginson, J. F. Archard and A. W. Crook, *Elasto-hydrodynamic lubrication*, Pergamon Press, 1977.